Variational Bias Correction in the NCEP's Data Assimilation System

Yanqiu Zhu*[1], John Derber[2], Andrew Collard[1], Dick Dee[3],
Russ Treadon[2], George Gayno[1], James A Jung[4],
David Groff[1], Quanhua Liu[5], Paul Van Delst[1],
Emily Liu[6], Daryl Kleist[2]

[1]*I.M. Systems Group, College Park, Maryland*
[2]*NOAA/NWS/NCEP/Environmental Modeling Center, College Park, Maryland*
[3]*European Center for Medium-Range Weather Forecasts, Reading, UK*
[4]*Cooperative Institute for Meteorological Satellite Studies, Madison, WI*
[5]*Joint Center for Satellite Data Assimilation, College Park, Maryland*
[6]*Systems Research Group*
*Correspondence to: EMC/IMSG, 5830 University Research Ct., College Park, MD 20740; email: Yanqiu.Zhu@noaa.gov.

ABSTRACT

Efforts have been invested in enhancing the original radiance bias correction scheme in the Gridpoint Statistical Interpolation (GSI) Data Assimilation System at the National Centers for Environmental Prediction (NCEP). The enhanced scheme effectively consolidates the original two-step procedure into a single step variational procedure inside the GSI, along with the newly added capabilities of adaptive background error variances of the bias predictor coefficients, passive channel bias correction, and bias initialization.

A new emissivity sensitivity predictor term is also constructed to account for the land/sea difference, as the new Community Radiative Transfer Model (CRTM release 2.1.3) development improves the microwave sea surface emissivity model, which results in a larger OmF contrast between land and sea. The results show that the enhanced radiance bias correction with the new emissivity bias predictor works well with the new CRTM and provides additional significant forecast skill improvement. Both the enhanced radiance bias correction scheme and the CRTM release 2.1.3 are included in the upcoming NCEP's operational T1534 implementation.

A new strategy is also developed to expand the enhanced radiance bias correction scheme into the all-sky microwave radiance assimilation. Only the microwave radiance data with matched cloud information with the first guess are used for estimating the radiance bias predictor coefficients, while the radiance data with mismatched cloud information are bias corrected using the latest bias predictor coefficients available. The preliminary results indicate that this strategy removes the radiance bias effectively and at the same time preserves the useful cloud information.

1. Introduction

Radiance bias correction is an important and necessary step in assimilating radiance data, and several schemes have been developed in major Numerical Weather Prediction (NWP) centers during the past decade to address this issue, for example, the scheme implemented by Derber and Wu (1998) in the Spectral Statistical Interpolation (SSI) data assimilation system (Derber et al. 1991; Parrish and Derber 1992) and later in the GSI (Wu et al. 2002; Purser et al. 2003a, 2003b) at the NCEP; the scheme used at Met Office (Hilton et al 2009); the scheme developed by Harris and Kelly (2001) at the European Centre for Medium-Range Weather Forecasts (ECMWF), and later a variational scheme that includes both the scan angle and air-mass components (Dee 2004).

The original radiance bias correction scheme in the GSI is a two-step procedure. The scan angle bias correction component outside the GSI is computed as the time-averaged Observation-minus-First guess (OmF) of the radiance data, and the variational air-mass component is inside the GSI to allow this component to be estimated at the same time as the analysis control variables in the analysis system. Although the original scheme has been successfully applied to all

assimilated radiance data throughout these years, enhancement efforts have been motivated to address some of the known and suspected issues.

In this study, the enhanced radiance bias correction replaces the original two-step procedure by a single variational procedure, obtaining both the scan-dependent and air-mass dependent components along with the control variables within the GSI. This change simplifies the operational suite, and alleviates the possible opposite drifts of the two bias components.

One newly added feature is the adaptive background error variances of the radiance bias predictor coefficients. Combining with the modified pre-conditioning and a new bias initialization step in the GSI, this feature offers the GSI the capability to automatically detect any new, missing or recovery of radiance data and to initialize any new radiance data.

Another important new capability is the passive channel bias correction with a new approach formulated and implemented at the end of the analysis inside the GSI. This capability provides a very convenient way to obtain the bias estimate of any radiance data that are not used but monitored for future use, such as the data from Suomi National Polar-orbiting Partnership (NPP). More details of the enhanced radiance bias correction will be described in Section 2.

A recent development of the enhanced radiance bias correction is a response to the upgrade of the CRTM. Both are part of the upcoming operational T1534 Global Forecast System (GFS) upgrade. Since the upgraded CRTM release 2.1.3 improves the microwave sea surface emissivity model, a larger OmF contrast is observed between land and sea. An emissivity sensitivity predictor term is constructed to account for the land/sea difference. The combined performance of the enhanced radiance bias correction and the CRTM release 2.1.3 will be discussed in this paper.

The radiance data used so far in the operational GSI data assimilation system are clear-sky radiance data. Research studies are also actively engaged in the all-sky radiance assimilation. A new strategy is proposed to expand the enhanced radiance bias correction for the all-sky microwave radiance data.

This paper is organized as follows: A brief description of the enhanced radiance bias correction scheme in the GSI is given in Section 2, and the new emissivity bias predictor is described in Section 3. Experiment setup and results are discussed in Section 4. A new bias correction strategy for all-sky microwave radiance data is developed in Section 5, and finally the conclusions are given in Section 6.

2. Enhanced radiance bias correction algorithm

The radiance bias correction scheme originally used in the operational GSI is described in Derber and Wu (1998). It consists of an air-mass dependent component and a scan angle component, hence the observation operator $\tilde{h}$ for radiance data can be expressed as

$$\tilde{h}(\mathbf{x},\beta) = h(\mathbf{x}) + b^{air}(\mathbf{x},\beta) + b^{angle}, \tag{1}$$

where $\mathbf{x}$ is the model state or GSI control vector, and $h(\mathbf{x})$ represents the radiative transfer model. The original scheme is a two-step procedure: the scan angle component b^{angle} is updated outside the GSI, and the variational air-mass component b^{air}, which is a linear combination of N predictors (here $N = 5$), is updated within the GSI. The original five predictor terms include global offset, a zenith angle term, cloud liquid water (CLW), lapse rate convolved with the channel's weighting function, and the square of the lapse rate convolved with the channel's weighting function.

The enhanced radiance bias correction scheme incorporates the scan angle bias component into the GSI through a simple K-th order polynomial of scan angle ϕ. Since the original zenith angle predictor is no longer needed now, b^{angle} is expressed as

$$b^{angle} = \sum_{k=1}^{K} \beta_{N+k-1}\phi^k, \tag{2}$$

where the order of the polynomial (K) is commonly chosen as 3 or 4. Hence, the total bias can be written as a linear combination of a set of predictors $p_k(\mathbf{x}), k = 1, 2, ..., N + K - 1$, and $p_1 = 1$. Letting β_k denote predictor coefficients, we have

$$\tilde{h}(\mathbf{x},\beta) = h(\mathbf{x}) + \sum_{k=1}^{N+K-1} \beta_k p_k(\mathbf{x}). \tag{3}$$

These coefficients are estimated during the minimization of the cost function

$$J(\mathbf{x},\beta) = \frac{1}{2}(\mathbf{x}-\mathbf{x}_b)^T\mathbf{B}_\mathbf{x}^{-1}(\mathbf{x}-\mathbf{x}_b) + \frac{1}{2}(\beta-\beta_b)^T\mathbf{B}_\beta^{-1}(\beta-\beta_b) + \frac{1}{2}[\mathbf{y}-\tilde{h}(\mathbf{x},\beta)]^T\mathbf{R}^{-1}[\mathbf{y}-\tilde{h}(\mathbf{x},\beta)],$$

where $\mathbf{y}$ stands for observations; $\mathbf{x}_b$ and β_b are the first guesses for $\mathbf{x}$ and β, respectively; $\mathbf{B}_\mathbf{x}$ is the background error covariance for $\mathbf{x}$; and $\mathbf{B}_\beta$ the block-diagonal background error covariance for predictor coefficients, with $\mathbf{B}_\beta^{(j)} = diag(\sigma^2_{\beta_1,j},\ldots,\sigma^2_{\beta_N,j})$ for channel j ($j = 1, 2, ..., J$).

For the original radiance bias correction scheme, the error variances σ^2_β are specified as 10.0 for all predictor coefficients of all channels. In the enhanced bias correction scheme, a new approach is taken to adaptively update the background error variances by the approximations of the analysis error variances of the radiance bias predictor coefficients from previous analysis cycle. The analysis error covariance can be approximated by the inverse of the Hessian, and the Hessian with respect to the radiance bias coefficients, $\mathcal{H}_\beta$, is written as

$$\mathcal{H}_\beta = \mathbf{B}_\beta^{-1} + \mathbf{H}_\beta^T\mathbf{R}^{-1}\mathbf{H}_\beta, \tag{4}$$

where $\mathbf{H}_\beta$ is the partial derivatives of $\tilde{h}(\mathbf{x},\beta)$ with respect to β. Moreover, due to the close interaction between the quality control and the radiance bias correction, a quasi-mode based bias initialization step is added in the GSI. The combination of the adaptive background error variances and the new bias initialization step allows the system to detect any new/missing/recovery of radiance data and initialize any new data automatically.

The Hessian $\mathcal{H}_\beta$ is also used in the modified pre-conditioning to speed up the convergence of the GSI minimization. The original pre-conditioner $\mathbf{Z}$ is in the form of

$$\mathbf{Z} = \begin{bmatrix} \mathbf{B}_\mathbf{x} & 0 \\ 0 & \mathbf{B}_\beta \end{bmatrix}. \tag{5}$$

Following Dee (2004), the pre-conditioner of the radiance bias scheme is modified to take into account the contribution from the observations to $\mathcal{H}_\beta$. $\mathbf{B}_\beta$ is replaced by $\mathbf{M}_\beta$ in the modified pre-conditioner, where ${\mathbf{M}_\beta}^{-1} = \mathcal{H}_\beta$. For simplicity, only diagonal elements of $\mathbf{H}_\beta^T\mathbf{R}^{-1}\mathbf{H}_\beta$ are considered in the calculation of ${\mathbf{M}_\beta}^{-1}$ at each analysis cycle in the implementation. Furthermore, a constant α is multiplied to $\mathbf{B}_\mathbf{x}$ for further preconditioning the control variables $\mathbf{x}$ to make the convergence of the control variable $\mathbf{x}$ compatible with that of β. In our study, α is chosen as $1.0E-3$.

Another new capability of the enhanced radiance bias correction is the passive channel bias correction. The new approach we take is different from that of Dee (2004) at ECMWF. In the GSI, the bias correction of the passive channels is performed at the end of analysis, using the same bias correction algorithm for active channels but to fit to the newly generated analysis. Letting $\mathbf{x}_a$ denote the analysis, and $\mathbf{y}$ denote the passive channel data that pass the quality control including cloud detection for Infrared data, the predictor coefficients β can be obtained by minimizing the functional F

$$F(\beta) = \frac{1}{2}(\beta-\beta_b)^T\mathbf{B}_\beta^{-1}(\beta-\beta_b) + \frac{1}{2}[\mathbf{y}-\tilde{h}(\mathbf{x}_a,\beta)]^T\mathbf{R}^{-1}[\mathbf{y}-\tilde{h}(\mathbf{x}_a,\beta)].$$

This capability provides a very convenient and efficient way to obtain the bias of any new satellite data that are not used but monitored for preparation for future use, such as the radiance data from the NPP satellites. More details of the enhanced radiance bias correction can be found in Zhu et al. (2013).

3. New emissivity sensitivity predictor

With the ongoing efforts towards the upcoming operational T1534 GFS upgrade at NCEP in 2014, both the upgraded CRTM release 2.1.3 and the enhanced radiance bias correction scheme are included in the upgrade package. Since the enhancement developments of these two components are conducted separately and parallely, although each was tested separately and exhibited improvements over the operational GFS configuration (Liu et al. 2011; Zhu et al. 2013), attention needs to be paid to the compatibility and combined performance of the two major changes of the analysis.

A desirable feature that accompanies the latest CRTM, release 2.1.3, is a general improvement in the accuracy of sea surface field of view simulations for surface sensitive microwave channels. For example, when applied in the GSI, the variances and biases of first guess departures for AMSUA surface sensitive channels have in general been reduced relative to the application of a previous CRTM, release 2.0.5, over sea surfaces. This CRTM improvement is due to the replacement of an older Fast Microwave Emissivity Model (FASTEM), FASTEM-1, with a newer FASTEM, (FASTEM-5), in CRTM release 2.1.3. A particularly salient component of the FASTEM-5 Geometrical Optics (GO) theory is the accounting of interactions with small-scale sea surface waves (Liu et al. 2011). This accounting of small-scale waves was absent in FASTEM-1.

As the CRTM release 2.1.3 improves the variances and biases of OmF for microwave surface sensitive channels over sea areas, larger OmF differences between land and sea are observed (e.g., the upper panel of Fig. 1). On the other hand, the radiance bias correction scheme doesn't have a bias predictor designed to deal with the large land-sea contrast. This was not an issue previously with the small land-sea differences, however, when combined with the CRTM release 2.1.3, this creates a situation where, either the large OmF land-sea differences are dumped into other existing bias predictors, or the radiance data bias correction settles down somewhere in between the OmFs over land and the OmFs over sea, or both. Therefore, an emissivity sensitivity bias predictor is constructed as the following in the enhanced radiance bias correction to handle this issue:

$$p_{emissivity}(\mathbf{x},\beta) = \begin{cases} 0 & \text{if over sea,} \\ \frac{\partial T_b}{\partial \epsilon} & \text{otherwise.} \end{cases} \tag{6}$$

Here ϵ denotes emissivity, and T_b is the brightness temperature. This emissivity sensitivity predictor takes into account not only the OmF differences between land and sea, but also the surface sensitivity of each individual channel. This predictor basically has no impact on high-peaking channels. An example of window channel is shown in Fig. 1 for channel 1 of AMSUA from NOAA19 on 0Z Aug. 1, 2012. The OmF before bias correction is displayed in the upper panel. Many of the radiance data over land are with large negative OmF values, but most of the data over ocean have positive OmF values. The OmF after bias correction is shown in the lower panel, and it is seen that the bias is reduced for the data over both land and ocean, and the large difference between land and sea is not evident any more.

4. Experiment setup and results

In this Section, the combined performance of the two analysis changes, i.e., the enhanced radiance bias correction (thereafter referred to as ERBC in the figures) and the CRTM release 2.1.3, is assessed. A development version REL-4.2.0_alpha of the parallel GFS along with GSI r27269 and CRTM release 2.1.3 is used for the experiments conducted in this study. The analyses are performed every 6 hours. The early analysis cycle, GFS, is started 2.75 hours after the synoptic hour with the observation window [-3,2.5] around the synoptic hour, and is followed by a 192-hour forecast. In this study, the 192-hour forecast is only issued at 00Z. The late analysis cycle, GDAS, is started at 6 hours after the synoptic hour with the observation window [-3,3], and provides a 6-hour forecast to the next early and late analysis cycles as the first guess.

Experiments are performed for an arbitrarily chosen period from July 2 to August 27, 2012. The first eight days are set aside for system spin-up and to allow the radiance bias correction to stabilize, and hence are excluded from the calculation of subsequent statistics.

The control experiment **CTL** is the low resolution 3DVAR parallel GFS, in which the original two-step radiance bias correction scheme and the CRTM release 2.0.5 are used. A horizontal resolution of 254 spectral triangular truncation (T254) and 64 unequally spaced sigma layers (L64) in vertical are used for the GSI. The operational conventional and satellite data, within the real-time cutoff window, are used in this study. They include rawinsonde, aircraft observations; land and sea surface reports; Atmospheric Motion Vectors (AMV) from geostationary and polar orbiting satellites; GPS bending angle observations; radiance data from HIRS, AMSUA, MHS, ATMS, GOES, a 281 channel subset of AIRS, and a 616 channel subset of IASI; as well as ozone data from SBUV and OMI.

The experiment **CRTMonly** is the same as the control, except that the CRTM release 2.1.3 is used. The other two experiments **ERBSwCRTM** and **ERBSwCRTMn** are the same as **CRTMonly**, except that the enhanced radiance bias correction is turned on. Two modes are tested for the enhanced radiance bias correction scheme: the radiance data on the cross-track scan edges are included in **ERBCwCRTM** and are excluded in **ERBCwCRTMn**. The exclusion of the data on the scan edges, on one hand, decreases the data coverage, but on the other hand, since the data on the scan edges tend to have larger biases, it is beneficial to the fitting of the scan angle bias formula Eq. 2 to the radiance OmFs across the

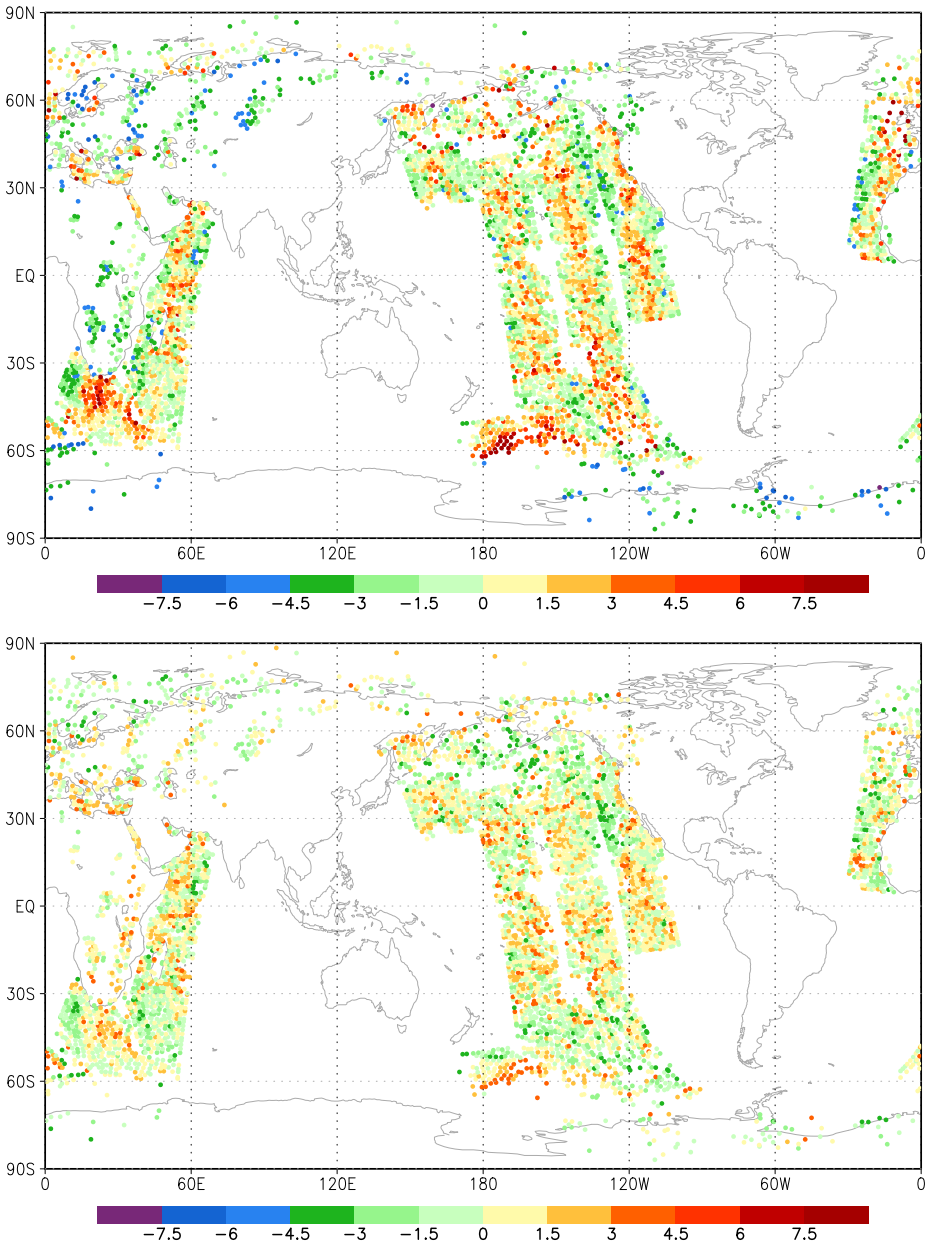

Figure 1. An example of OmF for AMSUA channel 1 data from NOAA19 at 00Z Aug. 1, 2012: before bias correction (upper), and after bias correction including the emissivity sensitivity predictor (lower).

scan angles. The impacts of the combined two analysis components (the enhanced radiance bias correction and the CRTM release 2.1.3) on the analysis and forecast are investigated in this Section.

First, let's take a look at the combined impact on the analysis. It has been known that our operational system has warmer temperature analyses over southern higher latitudes at lower vertical levels when compared with the ECMWF analyses. The warm bias was reduced from our separate experiments with each of the two upgraded components (Zhu et al. 2013). The combined effects of the two components are presented in Fig. 2, where the upper left panel shows the temperature analysis field at 700mb for the **CTL**, and the other three panels are the analysis differences between the experiments with respect to the **CTL**. The lower right panel is for the experiment **CRTMonly**, where only CRTM release 2.1.3 is used instead of the CRTM release 2.0.5; the upper right and lower left panels are for the experiments **ERBCwCRTM** and **ERBCwCRTMn**, respectively. The enhanced radiance bias correction is turned on in experiments **ERBCwCRTM** and **ERBCwCRTMn**, and the former includes the radiance data on the scan edges while the latter excludes the data on the scan edges. It is seen that the use of the CRTM release 2.1.3 reduces the warmer bias by about $0.2K$ at southern higher latitudes, but turning on the enhanced radiance bias correction on top of the CRTM release 2.1.3 further reduces

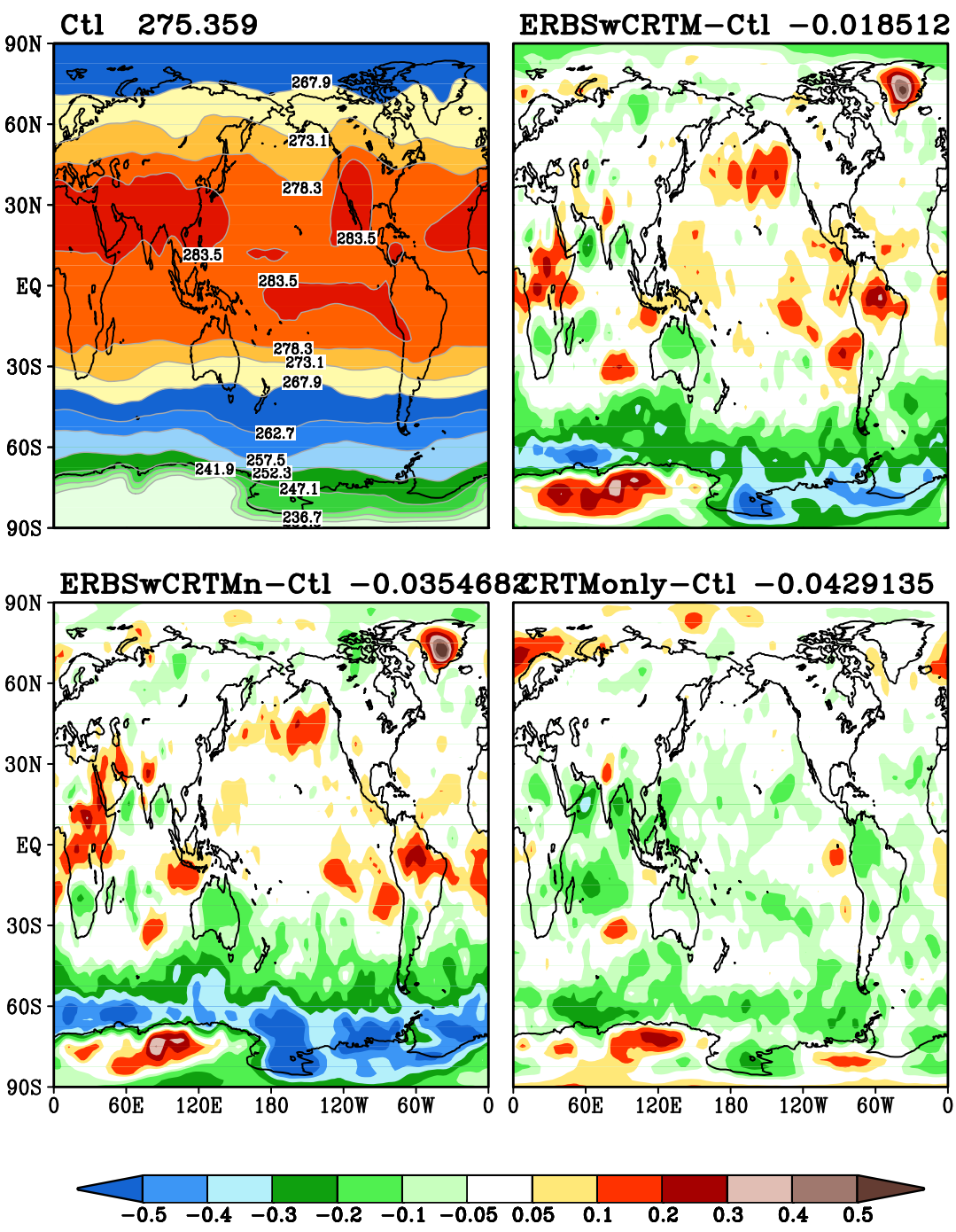

Figure 2. Mean temperature analysis field at 700mb for the **CTL** (upper left) and the analysis differences between each experiment and the **CTL** during the period from July 10 to Aug. 26, 2012: **ERBCwCRTM** (upper right), **ERBCwCRTMn** (lower left), and **CRTMonly** (lower right).

the magnitude of the warming (by as large as $0.5K$) and expands the cooling to much larger areas. The two modes of the scan-edge data usage exhibit similar patterns on the temperature analysis at 700mb, and slightly more cooling is observed in **ERBCwCRTMn**.

Regarding forecast skills, the anomaly correlation between the forecasts and their respective analyses is examined. The mean anomaly correlation of geopotential height at 500mb for the period from July 10 to Aug. 27, 2012 is presented in Fig. 3. It is shown that the impact of using the CRTM release 2.1.3 only (blue line) is neutral for the Northern

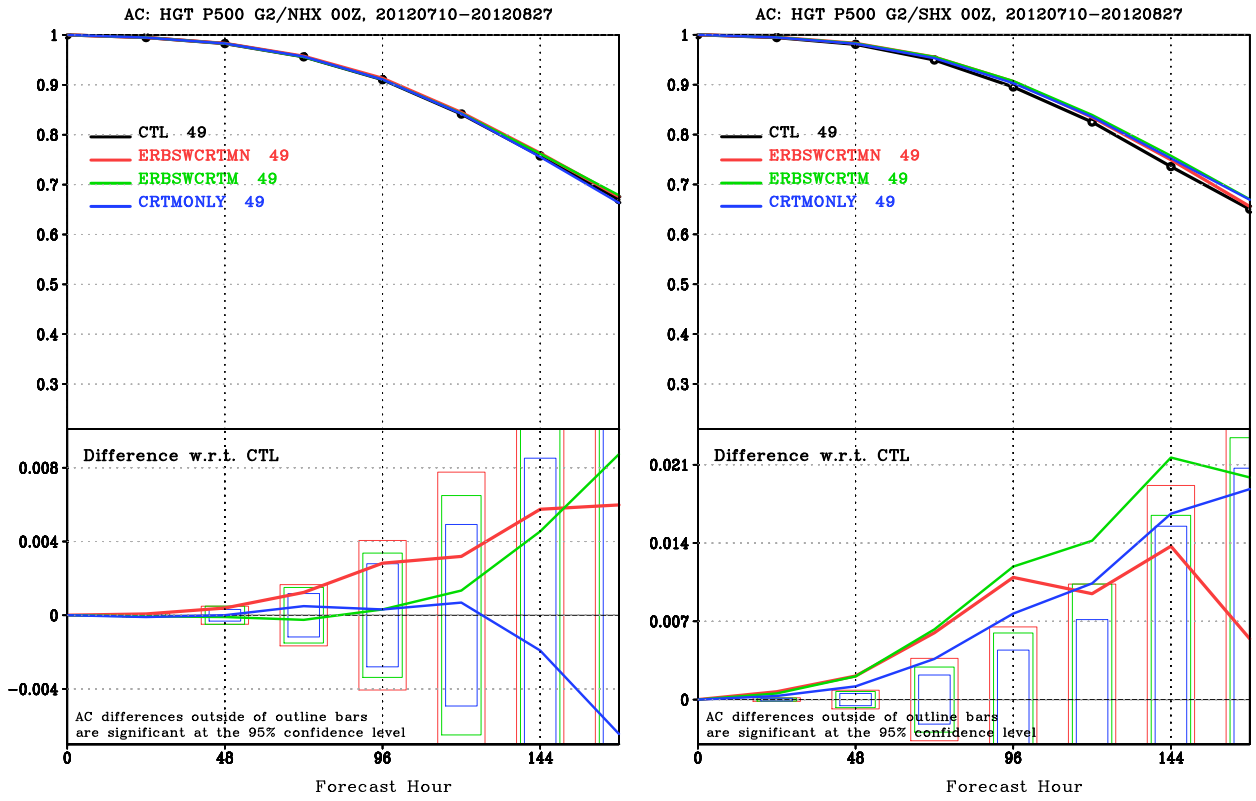

Figure 3. Mean anomaly correlation of geopotential height at 500mb for the Northern Hemisphere (left) and Southern Hemisphere (right) during the period from July 10 to Aug. 27, 2012.

Hemisphere, but positive in the Southern Hemisphere; After adding the enhanced radiance bias correction scheme on top of the CRTM release 2.1.3, the results of **ERBCwCRTMn** and **ERBCwCRTM** (red and green lines) exhibit better skill in the Northern Hemisphere and significant improvement of the forecast skill over the already improved Southern Hemisphere from **CRTMonly** (blue line).

The root mean squared error (RMSE) of vector wind at 200mb is also examined. The most significant improvements are observed over the Southern Hemisphere and in the Tropics. As reduced RMS errors are observed in all the three experiments in the Southern Hemisphere in Fig. 4, further reductions are obtained by the use of the enhanced radiance bias correction, especially the experiment **ERBCwCRTMn** where the data on the scan edges are excluded seems to perform better at the first two days than the other two. In the Tropics (Fig. 5), the enhanced radiance bias correction with the scan-edge data seems to erode the improvement obtained from the CRTM release 2.1.3, but the enhanced radiance bias correction without using the scan-edge data (**ERBCwCRTMn**) provides additional benefit to the improvement obtained from the CRTM release 2.1.3.

5. Expansion to the all-sky microwave radiance data assimilation

The results we present so far and the current operational GFS data assimilation system are for clear-sky radiance data assimilation. Research development efforts have been actively engaged in the all-sky microwave radiance data assimilation. For the assimilation of cloudy radiance data, cloud information from the forecast model and the observations are utilized in an effort to improve the analysis and model forecast over the dynamically important regions. Different approaches have been taken at the NWP Centers and research institutes: for example, the approach that doesn't involve a new cloud control variable but the use of cloudy radiance data help to improve the temperature and moisture fields at ECMWF (Bauer et al. 2010), and the approach that takes on one or several new cloud control variable(s) (e.g., at Met Office, English et al. 2006). The approach we have been testing for AMSUA data over ocean is to add a a total cloud water control variable (and the codes are also ready for separate cloud hydrometeors or total moisture as control variable(s), and comparison tests are underway). The background error covariance for the cloud variable(s) is obtained from both the static background error covariance and the ensembles through our 3DVAR/Ensemble hybrid system (Kleist et al. 2012)

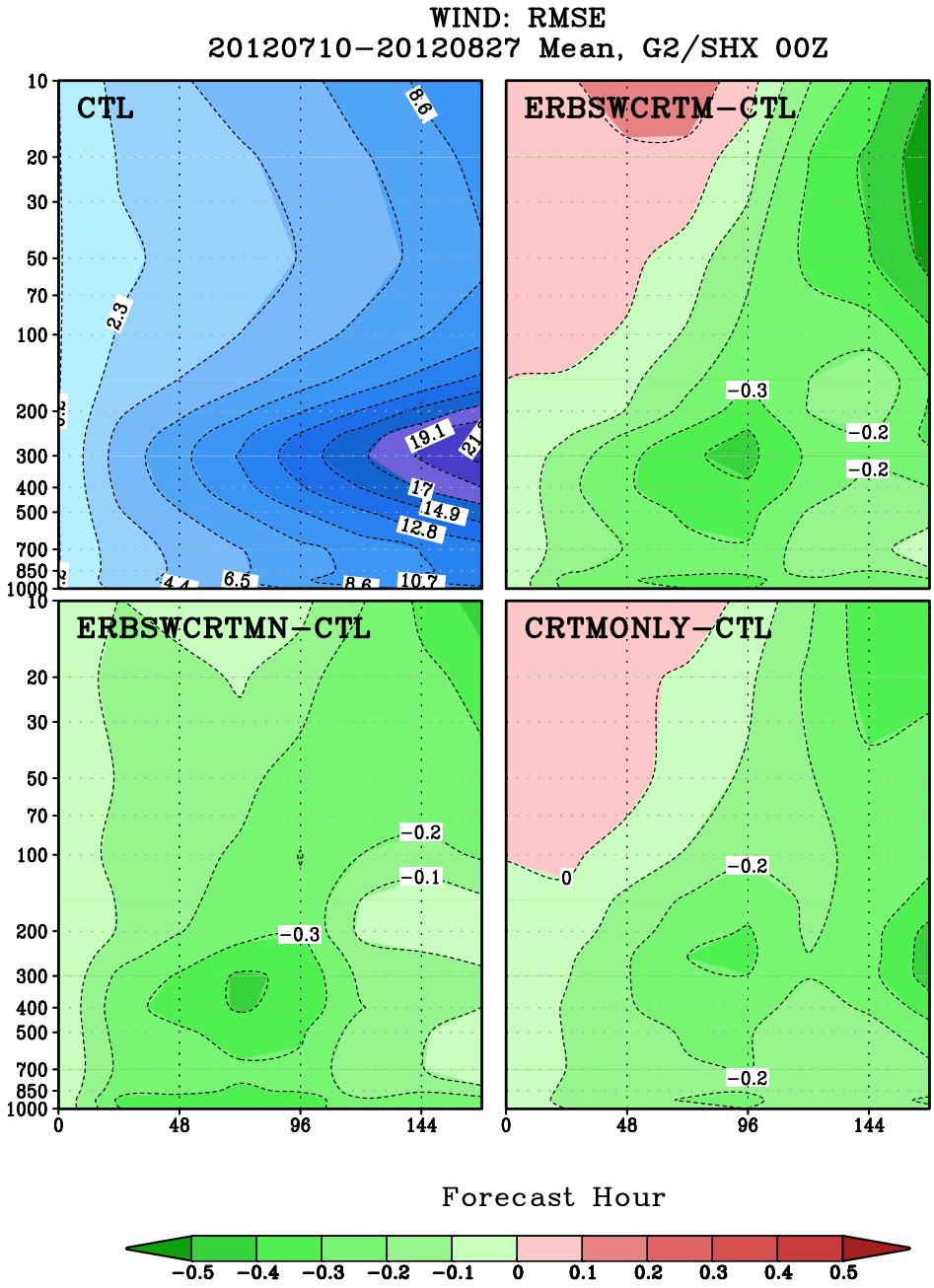

Figure 4. The RMSE of vector wind at 200mb for experiment **CTL** (upper left) in the Southern Hemisphere during the period from July 10 to Aug. 27, 2012, and the RMSE differences between **ERBCwCRTMn** (lower left), **ERBCwCRTM** (upper right), **CRTMonly** (lower right) and **CTL**, respectively.

with stochastic physics. For the quality control of the radiance data, the cloud filtering procedure, which is in place for clear-sky radiance assimilation to exclude the data that are affected by clouds, is no longer needed for all-sky microwave radiance assimilation. The observation error of the all-sky microwave radiance data is specified according to the averaged cloud liquid water values from the observation and the first guess (Geer and Bauer 2011), and the CLW over ocean is calculated as the following (Grody et al. 2001; Weng et al. 2003):

$$CLW = \cos\theta * \{c_0 + c_1 \ln[285 - T_b(1)] + c_2 \ln[285 - T_b(2)]\}, \quad (7)$$

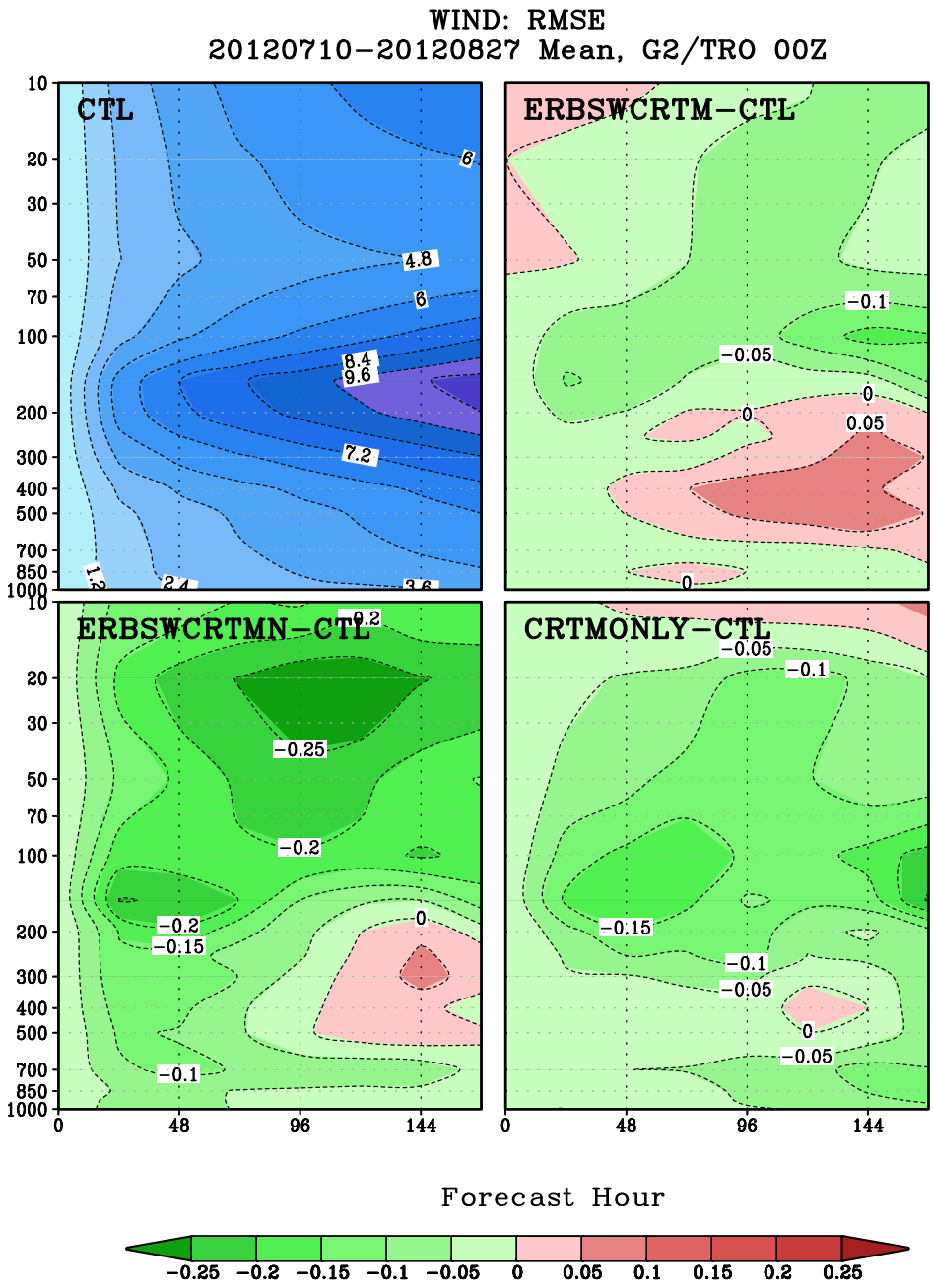

Figure 5. Same as Fig. 4 but for the Tropics.

where $T_b(1)$ and $T_b(2)$ are brightness temperatures for channels 1 and 2. We focus here on the radiance bias correction for the all-sky microwave radiance data. As the discussions and results presented in previous Sections are for clear-sky radiance data, a new bias correction strategy is proposed and tested for the all-sky radiance data in this Section.

5.1. New bias correction strategy

Before we get to the new bias correction strategy, we would like to review the role of the CLW bias predictor in the bias correction scheme. This predictor was constructed for clear-sky radiance data assimilation to remove the cloud signal from the cloud affected data. It is only applied to microwave radiance data over ocean. Because of the effectiveness of this predictor, the GFS operational system has been successfully incorporating some cloud affected radiance data with increased data coverage for the clear-sky radiance data assimilation. As we are working towards the all-sky radiance data assimilation, this term is no longer needed and set to be zero.

With the all-sky radiance data, the data can be categorized into four scenarios based on the two CLWs calculated from the observation and from the first guess: the two CLWs may indicate that both the observation and the first guess are clear-sky, or both of them are cloudy; Or the observation CLW points to cloudy but the first guess CLW points to clear-sky; or vice versa. The latter two categories are the locations where we expect to generate or eliminate cloud via the assimilation of all-sky radiance data. Our goal is to remove the bias from the radiance data while preserving the useful cloud information from the OmF with mismatched cloud information. That is, with proper sample of the radiance data, in a ideal situation after bias correction, we should see a Gaussian distributed OmFs of the radiance data with cloud information matched with the first guess, and one hump of the radiance data with mismatched cloud information on each side of the Gaussian distribution.

Since all bias coefficients of the enhanced radiance bias correction are obtained at the same time as the control variables during the GSI minimization process, and in this process all the OmFs of the quality-controlled radiance data are utilized in producing the analysis and the bias coefficients, it is likely that the OmF bias caused by the mismatched cloud information may get lost in this process and at the same time mess up with the bias correction of the radiance data that have matched cloud information with the first guess. To handle this difficulty, we propose a new strategy of bias correction for all-sky microwave radiance data: only the radiance data with cloud information matched with the first guess are used in the bias coefficients update at each analysis cycle; and the radiance data with mismatched cloud information are bias corrected using the latest bias coefficients available. Hence, the observation operator of the AMSUA radiance data can be written as

$$\tilde{h}(\mathbf{x},\beta) = \begin{cases} h(\mathbf{x}) + \sum_{k=1}^{N+K} \beta_{b_k} p_k(\mathbf{x}) & \text{if with mismatched cloud, over ocean,} \\ h(\mathbf{x}) + \sum_{k=1}^{N+K} \beta_k p_k(\mathbf{x}) & \text{otherwise,} \end{cases} \tag{8}$$

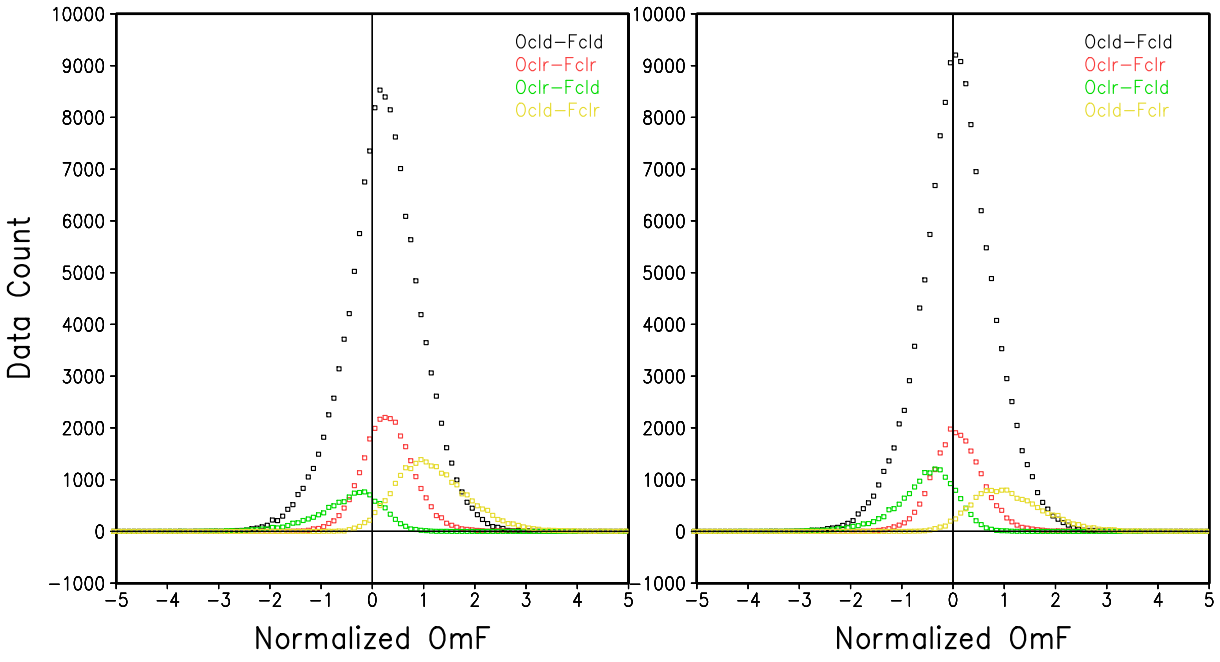

Figure 6. Histograms of two-week AMSUA channel 3 data from MetOp-A based on four cloud categories: the left panel is for the experiment without the new bias correction strategy for all-sky radiance data, and the right panel is for the experiment using the new strategy.

Preliminary experiments have been conducted to test the strategy with the GSI 3DVAR/ensemble hybrid GFS system. The resolution T254L64 is used for both GSI 3DVAR and the Ensemble Kalman Filter (EnKF) with 80 ensemble members. The observations used in the experiments are the same as the operational GFS run (i.e., clear-sky radiance assimilation), except that for AMSUA data over ocean, non-precipitating AMSUA radiance data are used in the experiments. An example of a two-week long statistics is given in Fig. 6 for AMSUA MetOp-A channel 3 to illustrate the effect of the new strategy. The bias-corrected OmF histograms of the four categories are presented in the figure with the left panel for the experiment without using the new bias correction strategy and the right panel for the experiment using the new strategy. It is seen that,

without the new bias correction strategy the histograms of the radiance OmFs with matched cloud information are pushed to right and the OmF biases become positive, while the corresponding two histograms after using the new strategy behave well and are centered around the bias zero line, and the other two categories with mismatched cloud information sit on the either side.

5.2. Scattering index bias predictor

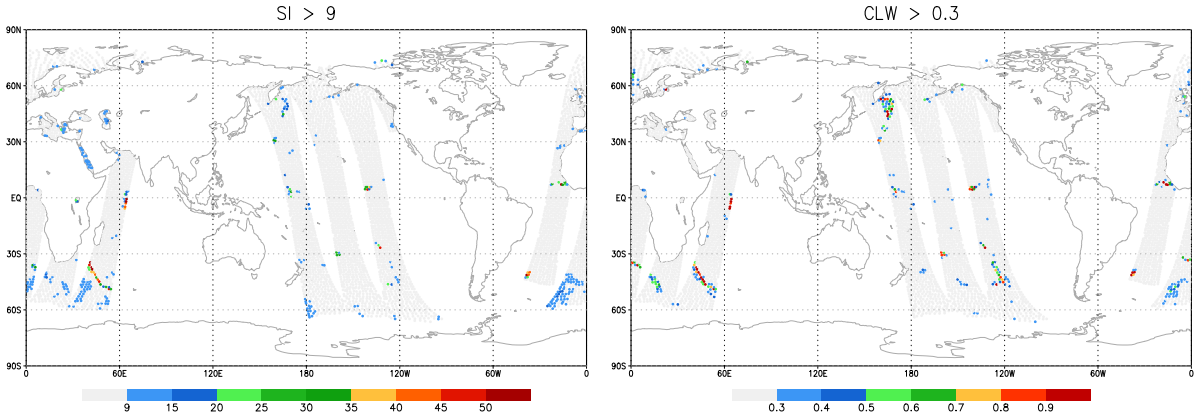

Figure 7. The scattering index SI (left) and CLW (right) for AMSUA data from NOAA19 at 00Z July 5, 2012.

Since precipitation vertical profiles are not currently made available for our first guess of the analysis because of file size issue, only non-precipitating radiance data are used in the previous subsection. This means that many cloudy radiance data will be passed by for now. One way to compensate the lack of first guess precipitation information, without losing precipitating radiance data, is to add a scattering index bias predictor to the enhanced radiance correction scheme. The scattering index SI is calculated as in Weng et al. 2003

$$SI = -113.2 + [2.41 - 0.0049 * T_b(1)] * T_b(1) + 0.454 * T_b(2) - T_b(15), \tag{9}$$

where $T_b(1)$, $T_b(2)$ and $T_b(15)$ are brightness temperatures for channels 1, 2 and 15. This predictor is set to be SI where observation indicates scattering, i.e., observation $CLW > 0.3$ or $SI > 9$; and this predictor is set to be zero everywhere else. From Fig. 7, the locations of $CLW > 0.3$ and $SI > 9$ generally agree well and complement to each other. The scatter plot of averaged CLW vs. OmF with bias correction for two-week AMSUA channel 1 data from NOAA19 is displayed in Fig. 8. The left panel is the experiment without the scattering bias predictor, and the right panel is the experiment with the scattering bias predictor. It is seen that the use of this bias predictor reduces the OmF bias at larger CLW bins.

This bias predictor experiment is simply used as a test of concept. We will shift our focus from non-precipitating to all ranges of cloud and precipitating radiance data once the precipitation information from the forecast model is written out for the analysis.

6. Conclusions and future work

Enhancement efforts have been made on the original radiance bias correction scheme. By combining the scan angle and air-mass bias components under the variational framework, the enhanced scheme replaces the original two-step scheme with a single step inside the GSI along with the control variables. Several other features are also added. First, a new scheme for updating the background error variances for the radiance bias coefficients is proposed and developed. Since the analysis error covariance can be approximated by the inverse of the Hessian, the background error variances are set to be the analysis error variances from previous analysis cycle. Together with the modified pre-conditioning that taking into account the observation contribution to the Hessian with respect to the bias predictor coefficients, and the new bias initialization step, the enhanced scheme is capable of automatically detecting any missing/new/recovery of radiance data and initializing the bias for any new radiance data.

Another new capability of the enhanced radiance bias correction is the passive channel bias correction. A new approach is formulated and implemented within the GSI when the new analysis is generated, by fitting the radiance bias correction

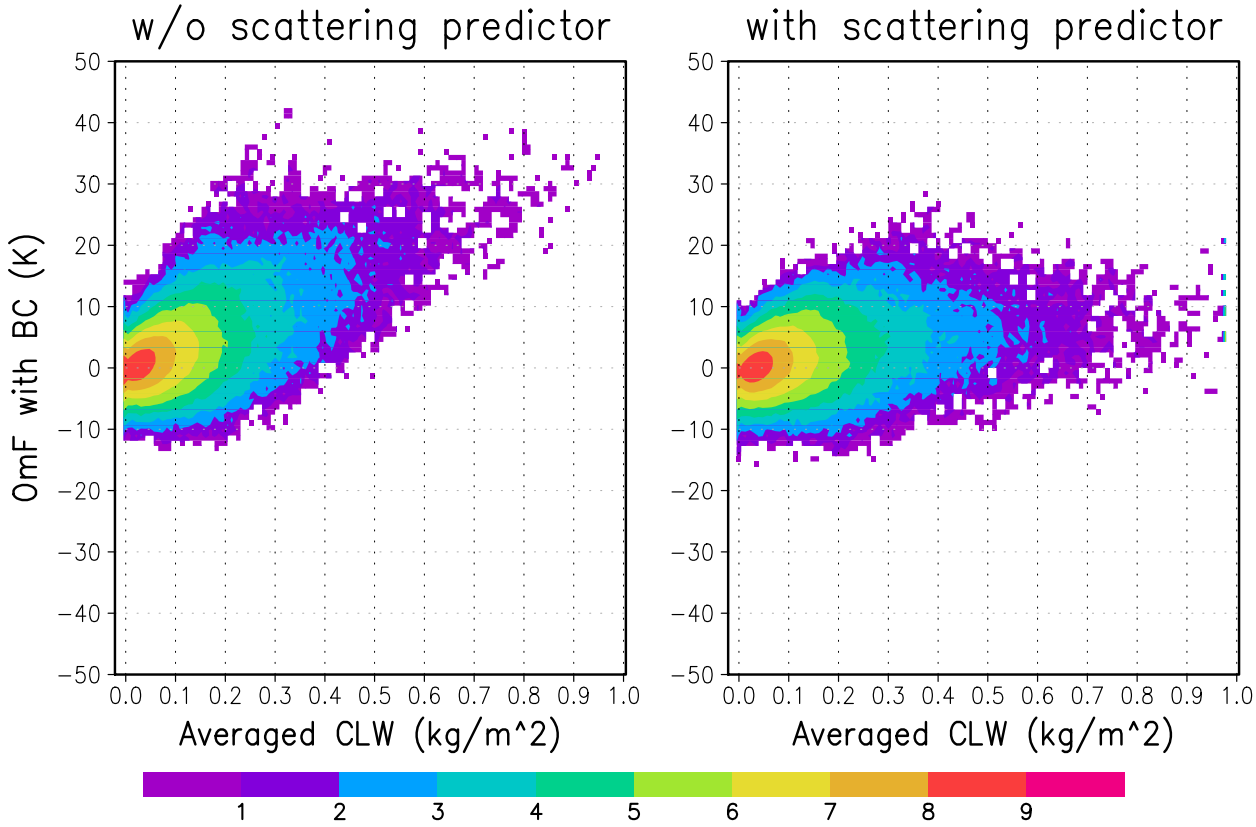

Figure 8. Scatter plot of averaged CLW vs. OmF with bias correction for two-week AMSUA channel 1 data from NOAA19: the left panel is the experiment without the scattering bias predictor, and the right panel is the experiment with the scattering bias predictor.

formula to the differences between the radiance observations and the newly generated analysis. This capability provides an efficient way to obtain the bias correction for any new and monitored radiance data. More detailed information about the enhanced radiance bias correction can be found at Zhu et al 2013.

A more recent development of the enhanced radiance bias correction is triggered by the upgrade of the CRTM. As the CRTM release 2.1.3 improves the microwave sea surface emissivity model, a larger OmF contrast is observed between land and sea. An emissivity sensitivity predictor term is constructed to account for the land/sea difference. Experiments are conducted to assess the combined performance of the enhanced radiance bias correction and the CRTM release 2.1.3, as both are included in the upcoming operational T1534 GFS upgrade. The results show that, while the CRTM release 2.1.3 improves the forecast skills in the Southern Hemisphere and the Tropics, the combination of the enhanced radiance bias correction and the upgraded CRTM provides further improvements in both Northern and Southern Hemispheres and the Tropics.

With the development of cloudy radiance assimilation in the GSI, how to perform bias correction for both clear-sky and cloudy radiance is yet another challenge. A new strategy is proposed in this study to obtain the bias predictor coefficients only using the radiance data with cloud information matched with the first guess, though all quality-controlled radiance data are used to obtain the analysis. The experiment results show that the strategy works well. A simple test is also done to examine the effectiveness of a scattering bias predictor on removing bias from the radiance data with a large amount of cloud liquid water. Since our data assimilation system is still evolving, especially with the model moist physics development, more experiments have to be done to carefully assess the performance of all-sky radiance assimilation.

References

P. Bauer, A. J. Geer, P. Lopez, and D. Salmond 2010. Direct 4D-Var assimilation of all-sky radiances. Part 1: Implementation. *Q. J. R. Meteorol. Soc.*, **136**, 1868-1885.

Geer, A. J., and P. Bauer 2011. Observation errors in all-sky data assimilation. *Q. J. R. Meteorol. Soc.*, **137**, 2024-2037.

Dee, D. P. 2004. Variational bias correction of radiance data in the ECMWF system. *Proceedings of the ECMWF workshop on assimilation of high spectral resolution sounders in NWP*, Reading, UK, 28 June - 1 July.

Derber, J. C., D. F. Parrish, and S. J. Lord 1991. The new global operational analysis system at the National Meteorological Center.. *Wea. and Forecasting*, **6**, 538-547.

Derber, J. C., and W.-S. Wu 1998. The use of TOVS cloud-cleared radiances in the NCEP SSI analysis system. *Mon. Wea. Rev.*, **126**, 2287-2299.

English, S., U. O'Keeffe, and M. Sharpe 2006. Assimilation of cloud AMSU-A microwave radiances in 4D-VAR. *The Proceedings of the 15th International TOVS Study Conference*, Maratea, Italy, 4-10 October 2006.

Hilton, F., N. C. Atkinson, S. J. English, and J. R. Eyre 2009. Assimilation of IASI at the Met Office and assessment of its impact through observing system experiments. *Q. J. R. Meteorol. Soc.*, **135**, 495-505.

Grody, N., J. Zhao, R. Ferraro, F. Weng, and R. Boers 2001. Determination of precipitable water and cloud liquid water over oceans from the NOAA 15 advanced microwave sounding unit. *J. Geophy. Res.*, **106**, 2943-2953.

Harris, B. A., and G. Kelly 2001. A satellite radiance-bias correction scheme for data assimilation. *Q. J. R. Meteorol. Soc.*, **127**, 1453-1468.

Kleist, D., K. Ide, J. Whitaker, J. C. Derber, D. Parrish, and X. Wang 2012. Expanding the GSI-based hybrid ensemble-variational system to include more flexible parameter settings. *AMS annual meeting*, New Orleans, LA.

Q. Liu, F. Weng, and S. English 2011. An Improved Fast Microwave Water Emissivity Model. *IEEE Transaction on Geoscience and Remote Sensing*, **49**, no. 4, 1238-1250.

Purser, R. J., W. Wu, D. F. Parrish, and N. M. Roberts 2003a. Numerical aspects of the application of recursive filters to variational statistical analysis. Part I: spatially homogeneous and isotropic Gaussian covariances. *Mon. Wea. Rev.*, **131**, 1524-1535.

Purser, R. J., W. Wu, D. F. Parrish, and N. M. Roberts 2003b. Numerical aspects of the application of recursive filters to variational statistical analysis. Part II: spatially inhomogeneous and anisotropic Gaussian covariances. *Mon. Wea. Rev.*, **131**, 1536-1548.

Parrish, D. F., and J. C. Derber 1992. The National Meteorological Center's spectral statistical interpolation analysis system. *Mon. Wea. Rev.*, **120**, 1747-1763.

Weng, F., L. Zhao, R. R. Ferraro, G. Poe, X. Li, and N. C. Grody 2003. Advanced microwave sounding unit cloud and precipitation algorithms. *Radio Sci.*, **38**, DOI: 10.1029/2002RS002679.

Wu, W. S., R. J. Purser, and D. F. Parrish 2002. Three-dimensional variational analysis with spatially inhomogeneous covariances. *Mon. Wea. Rev.*, **130**, 2905-2916.

Zhu, Y., J. Derber, A. Collard, D. Dee, R. Treadon, G. Gayno, and J. A. Jung 2013. Enhanced radiance bias correction in the National Centers for Environmental Prediction's Gridpoint Statistical Interpolation Data Assimilation System. *Q. J. R. Meteorol. Soc.*, DOI: 10.1002/qj.2233